A Virtual Patient Simulator Based on Human Connectome and 7 T MRI for Deep Brain Stimulation

Giorgio Bonmassar
Athinoula A. Martinos Center for Biomedical Imaging
Department of Radiology
Massachusetts General Hospital,
Harvard Medical School,
Charlestown, MA
Giorgio.bonmassar@mgh.harvard.edu

Leonardo M. Angelone
Office of Science and Engineering Laboratories,
Center for Devices and Radiological Health, U.S. Food and Drug Administration,
Silver Spring, MD
Leonardo.angelone@fda.hhs.gov

Nikos Makris
Department of Psychiatry and Neurology
Massachusetts General Hospital,
Harvard Medical School,
Charlestown, MA
nikos@cma.mgh.harvard.edu

***Abstract* — This paper presents a virtual model of patients with Deep Brain Stimulation implants. The model is based on Human Connectome and 7 Tesla Magnetic Resonance Imaging (MRI) data. We envision that the proposed virtual patient simulator will enable radio frequency power dosimetry on patients with deep brain stimulation implants undergoing MRI. Results from the proposed virtual patient study may facilitate the use of clinical MRI instead of computed tomography scans. The virtual patient will be flexible and morphable to relate to patient-specific neurological and psychiatric conditions such as Obsessive Compulsive Disorder, which benefit from deep brain stimulation.**

Keywords - VPS; DBS; OCD; MRI; CT; safety; specific absorption rate; SAR; heating.

I. INTRODUCTION

Many deep brain stimulation (DBS) patients may require regular MRI examinations throughout the course of their lives since MRI is often the diagnostic tool of choice for monitoring structural changes in the brain [1]. Whole-body MRI examination is used in many common injuries following accidents and comorbidities. Moreover, functional MRI could be potentially useful to assess the effects of electrical stimulation of the basal ganglia [2]. Because of safety concerns more than 300,000 per year patients with implanted leads (e.g., pacemakers, DBS, and catheters) are denied MRI [3]. One of the main concerns regarding use of MRI for DBS implants is related to potential radio frequency (RF) – induced heating [4][7]. The RF waves used in MRI to elicit signal from the tissue interact with the conductive leads generating potentially high induced currents along the leads ("antenna effect") and increased RF power deposition near the distal tip of the leads [8]. Unfortunately two cases of serious, permanent neurological injury related to the antenna effect of DBS leads during MRI were reported [9][10]. In one case, one patient with two bilateral implants underwent a routine MRI of the lumbar spine and reported a hemiplegia. The authors of the report associate the injury to the RF-induced currents generated by the body coil on the DBS implants, which produced an edema near one of the implants with the consequent paralysis [10]. Additionally, a case of neurological deficit (i.e., double-vision and severe right-sided motor contractions) in a patient with bilateral DBS leads who

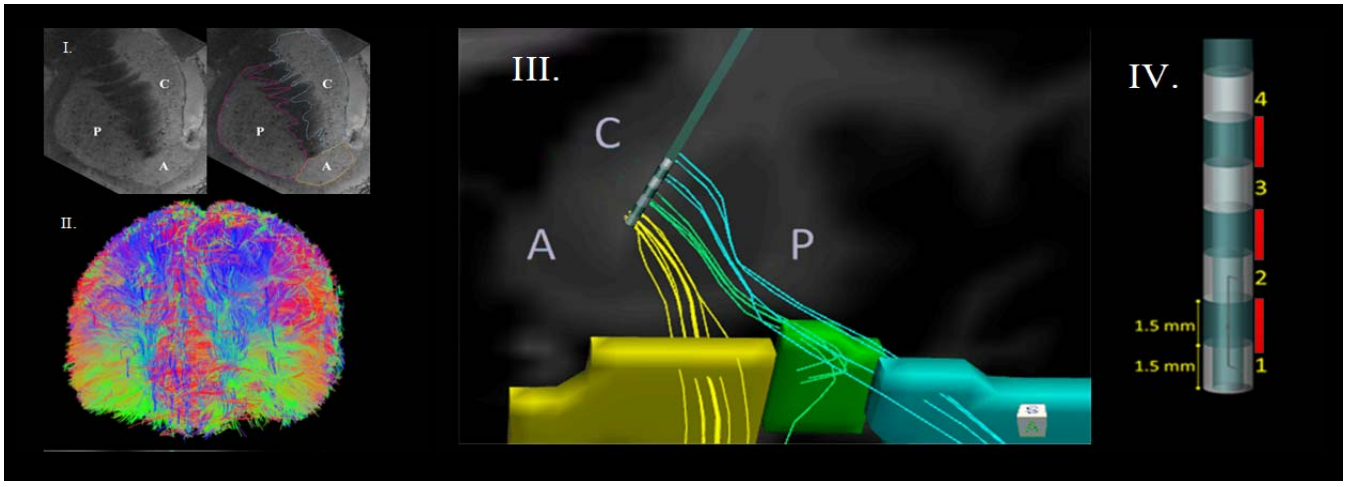

Figure 1: (I) Coronal section at the C.A.P. (Caudate-Accumbens-Putamen) level of a 7T high-resolution (100 μm^3 isotropic) ex-vivo human dataset showing detailed anatomy of the VC/VS target area (cross-hair in red) within the anterior limb of the internal capsule. (II) DSI connectome data set. The Connectome MRI data (voxel size: 2 × 2 × 2 mm^3) could be reliable in identifying the fiber tracks for connecting OCD targets, (III) electrode placement in the VC/VS target area traversed by fibers (yellow fibers) of the ventromedial prefrontal-basal ganglia tract at the C.A.P. coronal slice. The latter fibers stem from the ventromedial prefrontal area (yellow block). (A=nucleus accumbens, C=caudate nucleus, P=putamen), (IV) Model of the implanted DBS electrode.

underwent diathermy was also reported [11]. Recently Shrivastava et al. reported temperature increases up to 30°C in the tissue near DBS electrodes implanted in suine undergoing high field MRI (i.e., 9.4 Tesla) [12]. Based on guidelines approved by the U.S. Food and Drug Administration (FDA), in the US MRI can be used in DBS patients with very specific conditions [13]. For example, it is possible to scan patients with DBS implants only with a transmit head coil. Also, the use of 3T MRI systems, including the state-of-the-art MRI multichannel transmit coils, is contraindicated.

Computational models have been used as a supporting tool to evaluate RF-dosimetry in MRI. Numerical DBS models are based on a wire or set of wires, which represents the virtual DBS implant, superimposed to healthy human brain models [8][14]. Several numerical models for electromagnetic analysis of DBS have been proposed [15][20]. Recently, anatomically precise head models with implanted DBS leads with a multiscale resolution up to $0.2mm^3$ isotropic were also developed [8][21]. The models were based on Finite Difference Time Domain (FDTD) simulations. FDTD models have been validated in the past against temperature measurements, showing an accuracy of 20% as predicted by the bioheat equation [22] with respect to whole-body specific absorption rate (SAR). The DBS models described above allowed for accurate geometrical modeling of implanted leads as well as precise computation of 1g- and 10g-averaged SAR. Nevertheless, the models were characterized by a limited precision with respect to anatomical modeling of the structures involved in the stimulation, anisotropic dielectric constants, information about head perfusion, and the tissue scar from the surgery.

The rest of this paper is organized as follows. Section II describes the significance of the different tools used for the modeling. Section III describes the methods used. Section IV presents the results. Section V includes the discussion. The acknowledgement and conclusions close the article.

II. Background And Significance

A. Importance of structural MRI-based modeling

Neurocircuitry models of Obsessive-Compulsive Disorder (OCD) pathophysiology are currently supported by neuroimaging studies indicating the critical role of abnormal frontal-basal ganglia–thalamic circuits (cortico-striato-thalamo-cortical or CSTC circuitry). The most relevant anatomical structures involved are the orbital frontal cortex (OFC), anterior cingulate cortex (ACC), the ventral striatum and medial thalamus. It has been reported that in OCD fiber tracts connecting these centers may be abnormal [23] and that ablating or modulating these white matter pathways (e.g., in anterior cinglulotomy or anterior capsulotomy) as well as DBS on the Ventral Capsule/Ventral Striatum (VC/VS) may be associated with therapeutic improvement [24]. The VC/VS in the Anterior Limb of the Internal Capsule (ALIC, which is approximately 20 mm long in its dorsoventral extension and 2-5 mm wide mediolaterally at the coronal sections where the nucleus accumbens is present) is currently a target for DBS in OCD (Medtronic, Minneapolis, MN) (Fig.1). More specifically, a small fiber tract connecting the ventromedial prefrontal cortex (vmPFC) with the medial thalamus, basal ganglia and brainstem (vmPFC-BG) is thought to be a central to OCD pathophysiology and treatment response. The latter is a relatively small fiber bundle, of about 2 mm in diameter, which courses approximately 4-5 mm above the nucleus accumbens septi interconnecting ventral prefrontal cortex with basal ganglia, thalamus and the brainstem [24]. Given the increased clinical practice and efficacy of DBS in OCD, the accurate anatomical characterization of this surgical target in terms of its precise location, relative topography with surrounding structures (in particular with the nucleus accumbens septi and the anterior commissure) and size represents an important goal for numerical models – such as the Virtual Patient Simulator described herein– for DBS modeling.

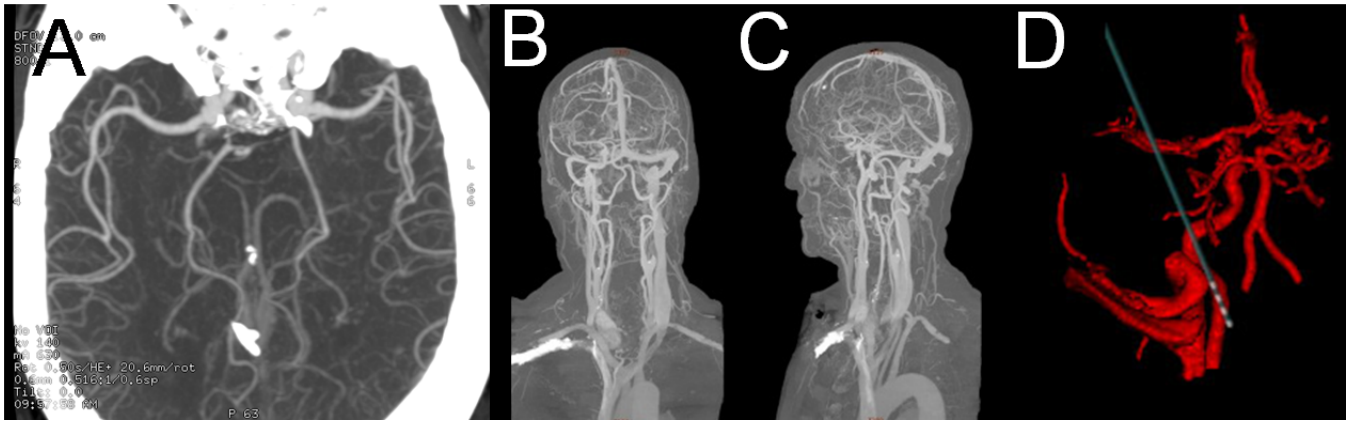

Figure 2: (A-C) Images of CTA acquired at the Radiology Department at MGH with 600μm in plane resolution, (B,C) 3D reconstruction with bone subtraction using dual energy CTA. (D) Illustration of how vasculature may wrap around an electrode.

B. Importance of Connectome-based modeling

Anisotropy of electrical properties of tissue arises in nerve and muscle fibers which consist of bundles of long, parallel myelinated elements. The VPS model described here will include Diffusion Tensor Imaging (DTI) data, to model tissue anisotropic conductivity [25]. To generate the model, the acquired diffusion tensor **D** will be converted into a complex relative permittivity tensor $\boldsymbol{\varepsilon}^*$ using a simple linear transform $\boldsymbol{\varepsilon}^* = \frac{\varepsilon^*}{d} \cdot \mathbf{D}$, where ε^* is the tissue complex relative permittivity [26] and d is the diffusivity.

Preliminary data (Fig. 1.B) show that Connectome MRI data (voxel size: 2 × 2 × 2 mm^3) may be reliable in identifying the fiber tracks connecting vmPFC and BG. The gradient strength determines the sensitivity, accuracy, and resolution of diffusion imaging. Data were acquired with a new Connectome scanner, installed at the A. A. Martinos Center, Massachusetts General Hospital, purpose-built for diffusion MRI with ultra-high gradients of 300 mT m^{-1}. As shown by a recent study [27] this technology allows for enhanced sensitivity and resolution of white matter imaging and MRI tractography of 5-10 fold over any other human DTI or High-Angular Resolution Diffusion Imaging (HARDI) such as the Diffusion Spectrum Imaging (DSI) technology. Fiber tracks were generated by using spatial information derived from high spatial resolution ex-vivo diffusion imaging (voxel size: 100 µm isotropic). .

C. Importance of Computed Tomography Angiography (CTA)-based modeling

Heat transport in biological tissues, which is usually expressed by the Pennes bio-heat equation, is a complex process that involves thermal conduction in tissues, convection and perfusion of blood (delivery of the arterial blood to a capillary bed in tissues). The underlying assumption of lack of perfusion used for many in vitro studies is often considered as a worst-case scenario for temperature changes at the distal tip and related tissue injury. However, a more accurate solution may be computed by solving the partial differential bioheat equation [28]:

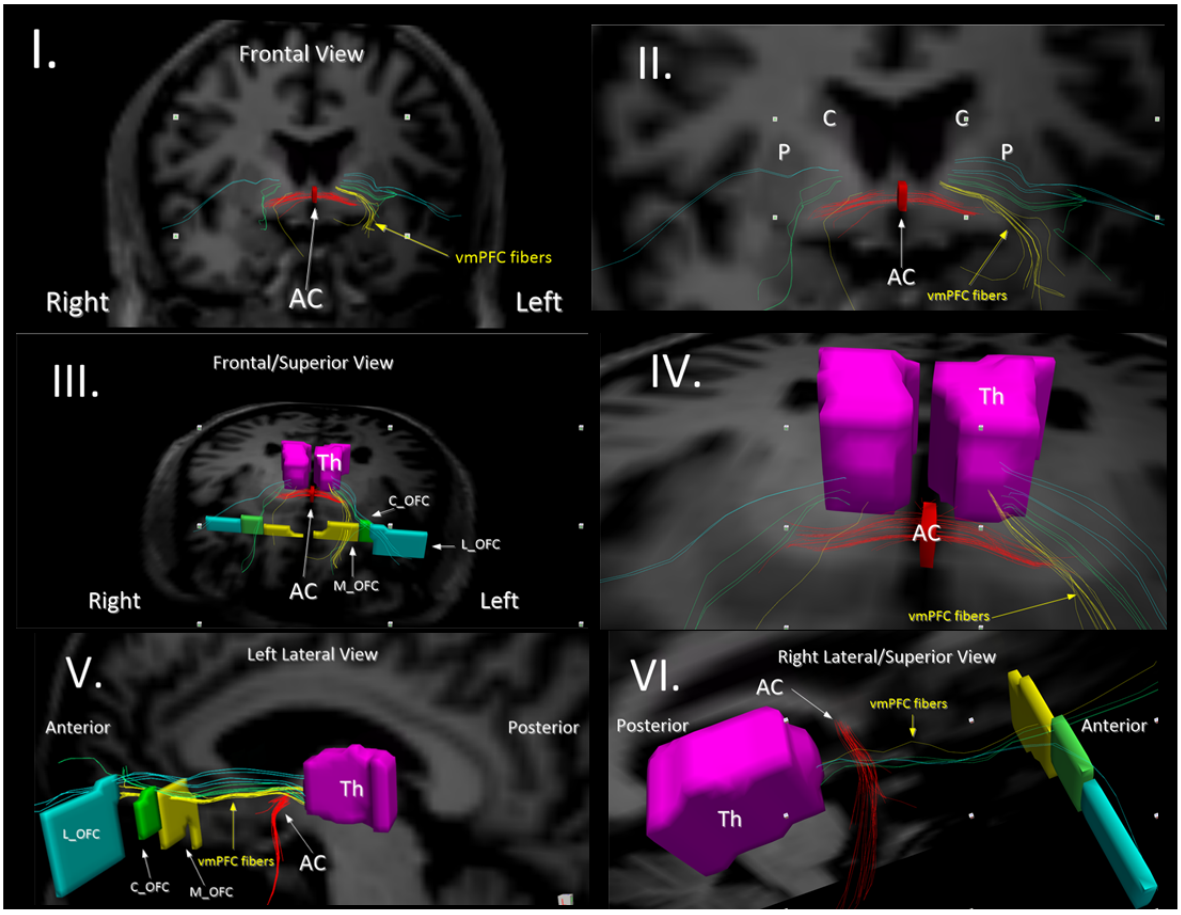

Figure 3: 3D reconstructions of ventromedial prefrontal (vmPFC) fibers and the anterior commissure (AC) from DSI connectome data of an individual subject (same as Fig. 1). Frontal (I., II, III, and IV) and lateral (IV and V) views showing vmPFC fibers connecting different regions of the orbital frontal cortex (lateral L_OFC, medial M_OFC and central C_OFC orbital frontal cortex) with the thalamus (Th). The vmPFC fibers are located dorsal to AC as shown in zoomed views (II and IV). Other abbreviations: C = caudate nucleus and P=putamen.

$$\rho C_p \frac{\partial T}{\partial t} - \nabla \cdot (k \nabla T) - M(T) + P(T)(T - T_B) + R_L(T) = 2\rho\, SAR \quad (2)$$

Where **ρ** is the mass density [kg/m^3], C_p is the heat capacity [J/(kg °C)], ∇T the gradient of temperature [°C], **k** is the thermal conductivity [W/(m °C)], **M** is the metabolic heat production [J/(s m^3)], **P** is perfusion parameter [J/(s °C m^3)] which becomes the heat loss when multiplied by the difference between the tissue temperature (T) and the blood temperature (T_B), $\mathbf{R_L}$ is the respiratory heat loss [J/(s m^3)], and ***SAR*** is the local specific absorption rate [W/kg] in the tissue generating the Joule heating. Bold symbols indicate vector fields or space dependent quantities (e.g., mass density is spatially variant, as it depends on the particular tissue [29]. The anatomical head model can be improved by including a realistic vascular structure and studying its thermal effect of perfusion and estimation of perfusion parameter (**P**) in the bioheat equation (eq.2). The realistic vasculature can be extracted from CTA images (Fig. 2).

D. Importance of Tissue Scaring around the DBS Electrode

Chronically implanted recording electrodes provoke an immune reaction against them. The histopathological finding is that of gliosis and spongiosis around the electrode track, which forms an encapsulation layer referred to as the "glial scar". This reactive glial tissue which surrounds the implanted electrodes is approximately 200 μm thick and progressively isolated the electrode from surrounding neurons modifying the electric field and acts as a natural neuro protector against heating of the electrode tips. The conductivity and permittivity of the scar tissue can be modelled at the frequency of interest (e.g., 128 MHz for a 3T MRI system) as a ring around the electrodes. The scar tissue will affect the bio-heat modeling behaving as a thermal insulating shield, thus improving the accuracy of the model.

E. Impact of the new RF pulse

The issue of heating of implants during MRI has been studied for several years [30] and analytical solutions (e.g., Green's function) to the problem have been proposed for simple geometries. Modifications of the implant leads and wires for reducing the RF-induced heating have been proposed introducing chokes or special geometrical paths of the wire. However, design modifications may be not appropriate for patients who already have DBS implants, since replacing the original leads with new leads requires major brain surgery. Because RF heating depends on the MRI RF transmit field, recent studies have focused on the modification of the transmit field in order to minimize the electric field in and around the implant and thus reducing the RF-induced heating near the implant.

III. METHODS

The study is based on *ex-vivo* analysis of collected 7 Tesla (7T) T2* and Connectome diffusion MRI data.

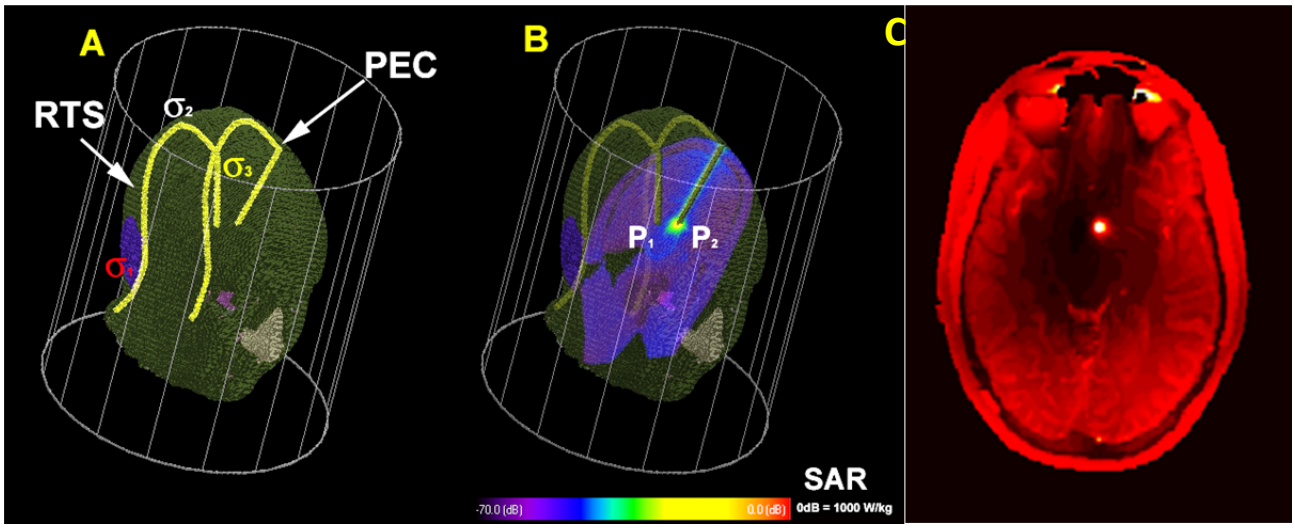

Figure 4: (A) Human head model with prototype of RTS and PEC implant (B) Computed SAR for the head model and the two implants. The 1mm^3 SAR at the tip of the RTS lead (P_1) was five –order of magnitude lower compared to SAR at the tip of PEC lead (P_2) (C) Results of electromagnetic simulations showing a high energy deposition near the distal tip of a monolateral metallic DBS lead.

A. Overview of study design, data acquisition and analysis.

(a) *Structural T2* 7 Tesla MRI data* The model is generated by segmenting 21 different brain structural entities on the *ex-vivo* structural MRI, as well as 28 non-brain structural entities following the approach described in Makris and colleagues [29]. The new head model now contains both the PD and the OCD targets found using tractographic methods. This *ex-vivo* brain consisted of MRI data of a hemisphere fixed in Periodate-Lysine-Paraformaldehyde (PLP) using the following parameters: T2*-W, 100 μm^3 isotropic resolution,

TR/TE/flip=40ms/20ms/20°, 1600×1100×896 matrix. Segmentation of OCD-DBS target-related cerebral structures – specifically the putamen, caudate nucleus, nucleus accumbens and anterior limb of the internal capsule – were manually outlined (on a re-sampled dataset at 1 mm isotropic spatial resolution of the original *ex-vivo* high-resolution – 100 μm^3 isotropic resolution – dataset acquired at 7 Tesla) using the segmentation methods by Filipek [31] and Makris [32], which have been developed and validated at the MGH Center for Morphometric Analysis, and have been implemented in several clinical studies.

The VC/VS in the ALIC is currently a target for DBS for OCD. It was approved in 2009 by the FDA with a Humanitarian Device Exemption (HDE) [33]. Importantly, a structure within this large territory, namely the vmPFC-BG tract is thought to be a more specific target for this procedure in OCD. Even though this is a relatively small fiber bundle, the ALIC/VS was segmented as follows by reaping the benefits of the high-resolution dataset.

(a) The anterior limb of the internal capsule is delimited medially by the head of the caudate nucleus, laterally by the putamen and ventrally by the nucleus accumbens. These structures were delineated by direct visualization using intensity-based contours in the Cardviews software system.

(b) *Connectome DSI data* were acquired on the Connectome 3T scanner using Gmax = 300 mT/m. This data acquisition was done on a 64-channel coil array using a single refocused spin echo sequence with the following features: TR = 2800 ms, TE = 56 ms, 63 axial slices, FOV = 220 mm, R = 3 GRAPPA, 2.0 mm isotropic resolution (BW = 2390 Hz/px), b = 15,000 s/mm^2. These data were

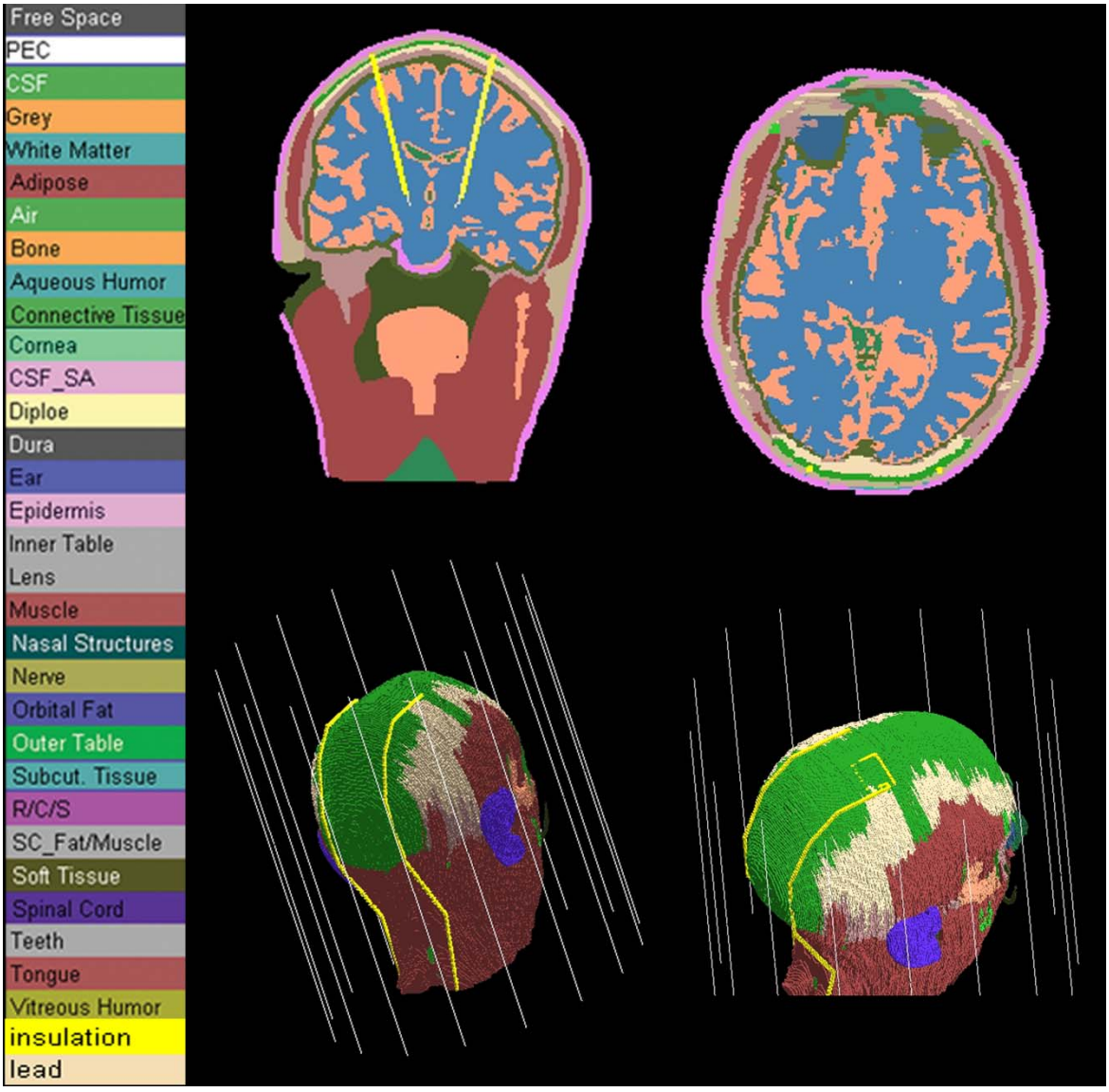

Figure 5: Anatomically fine-grained head model with a co-registered intracranial implant (white) and insulation (yellow). The coronal view show the 29 tissues manually segmented. The corresponding color code for each tissue is to the left of the image. (Bottom Left) 3D view of the head model and DBS implant, where external tissues (epidermis and subcutaneous tissue) have been removed for illustrative purposes.

transformed into DTI data to estimate complex relative permittivity tensor introduced in eq. (1). The vmPFC-BG tract was delineated using diffusion Connectome data as shown in Fig. 1.II. DTI/DSI data were visually validated by comparing the computed fiber tracks with anatomical atlases giving particular emphasis to the basal ganglia region as shown in Fig. 1.I. Furthermore, DTI/DSI data provided detailed information on the fiber tract connectivity between the ventromedial prefrontal cortex, basal ganglia, and thalamus. The latter is useful for DBS programming [35] and basic neuroscience research.

IV. RESULTS

In the model preliminary developed, the OCD target structures for DBS were identified and segmented using high-resolution T2*-W, diffusion spectrum MRI data, and electromagnetic simulations for MRI safety.

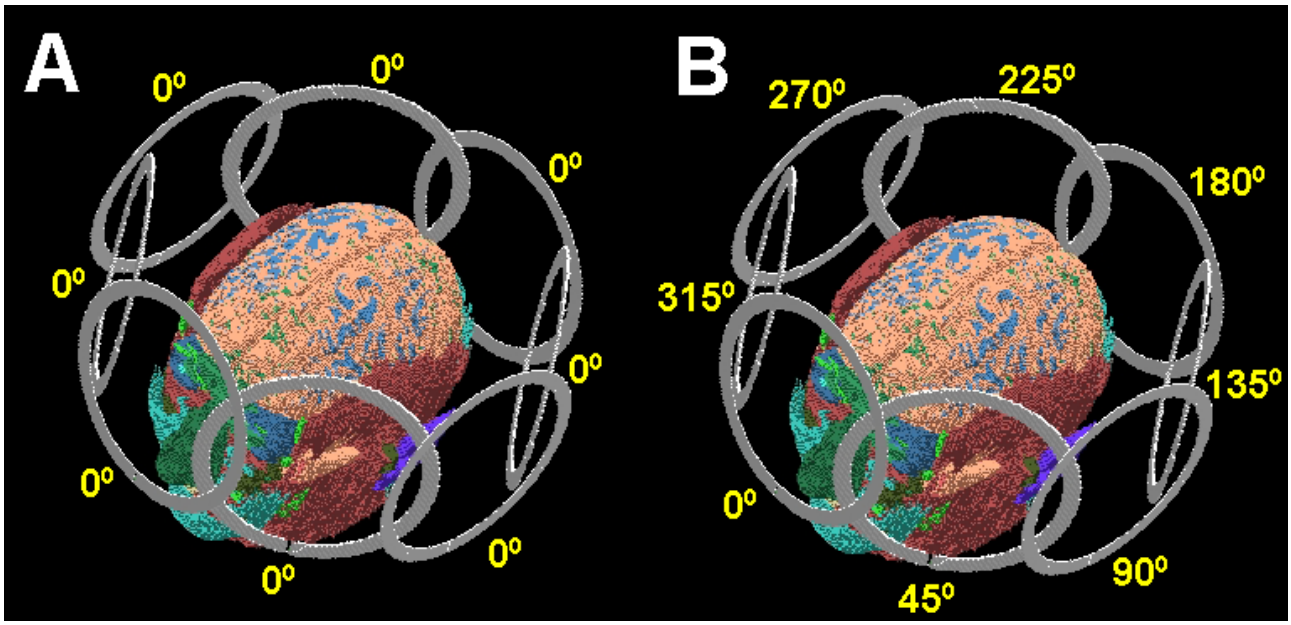

Figure 6: Geometrical model of the coil array and our model [29] with examples of null (A) and uniform (B) eight-channel transmit phase array vectors [34]. .

B. Numerical Model of Deep Brain Stimulation implant

A high-resolution model was generated based on the MRI data by distinguishing twenty-one brain [31] and twenty-eight non-brain anatomical structural entities. Each of the anatomical structural entities was associated to an electrical structural entity with electrical properties defined according to the literature [36][37]. The overall head dimensions were 170 mm in width, 217 mm in depth, and 238 mm in height and the total volume of the head model was 4,642,730 mm^3. The model was used for RF dosimetry studies of clinical significance [8], including preliminary studies with DBS implants. Two bilateral implants were modeled as insulated wires connected to the left and/or right targets in the head [10]. The wires were modeled as a perfect electric conductor (PEC) and the dielectric was modeled as Teflon. A four-electrode connection [35] was also modeled in full detail reaping the benefits of the high spatial resolution (Fig. 1).

Fig. 3.I and 3.II show data from a manual segmentation procedure to outline the different anatomical structures related to the VC/VS target area derived from a high-resolution 7 Tesla dataset and DSI-based tractography. Furthermore, the fiber connections between the orbital frontal cortex and the thalamus were reconstructed tractographically, visualizing them in relation to the anterior commissure (AC) to elucidate the spatial relationships between these fiber tracts. Fig. 3 shows that the vmPFC fibers – connecting different regions of the orbital frontal cortex (lateral L_OFC, medial M_OFC and central C_OFC orbital frontal cortex) with the thalamus (Th) – follow a pattern of spatial organization. Specifically, in the orbital frontal region within the anterior limb of the internal capsule they verticalize from a lateral to medial horizontal deployment showing the following spatial distribution above the nucleus accumbens. The L_OFC fibers are more dorsal, the M_OFC ones are more ventral and the C_OFC fibers are in-between. With respect to the AC, vmPFC fibers are located dorsal to AC as shown in zoomed views (Fig 3.II and 3.IV).

Fig. 4 shows an example of the numerical head model with implanted DBS leads modeled as resistive tapered stripline (RTS) [38] or metallic (PEC) wires. The model allowed simulating the high local SAR near the PEC lead as well as the lower local SAR near the tip of the RTS lead.

Values were normalized to obtain a whole-head averaged SAR of 3.2 W/kg [10][39][40].

Additionally, dual energy CTA images with bone subtraction (Fig. 2.B and 2.C) were performed using standard contrast agents. Segmentation was obtained by standard thresholding [41] from the images containing enhanced vascular information validated by comparison with vascular atlases [42][44]. These data may be used to inform more precise thermal analysis and prediction of thermal response of target nuclei surrounding the DBS electrode exposed to RF energy (Fig. 2.D).

V. DISCUSSION

Clinical work in OCD indicates that several compulsive behaviors in this disorder are related to avoidance of putative dangerous situations. The neural system that mediates avoidance is the same one that also underlies reward-seeking and comprises anterior cingulate/orbital frontal connections. Currently, neurosurgical procedures such as anterior cingulotomy, subcaudate tractotomy (SCT) and DBS are offered as an option to reduce symptom severity and increase quality of life in cases of medically intractable OCD. Given that 40-60% of patients with OCD do not have satisfactory response to optimal management [45], these procedures have been used for therapeutic benefit with very positive outcomes [46][49]. At Massachusetts General Hospital it has been recently shown that in 73% of these patients symptomatology was improved [50][51]. DBS is a therapeutic procedure aiming to change activity in fronto-basal ganglia circuits by injecting electrical stimulation in the Ventral Anterior Internal Capsule (VA-ALIC) and adjacent Ventral Striatum (VS), (i.e., nucleus accumbens septi). Given the efficacy of DBS and CST in cases of medically intractable OCD, an understanding of the disrupted connectivity is important to elucidate OCD psychopathology and provide guidance in making the SCT lesion or the DBS target more effective. Current Connectome and 7 Tesla MRI technology allows for more precise characterization of these targets for therapeutic intervention and of their relative topography.

There have been reports of serious accidents associated with MRI-related heating [10]. However, OCD patients with DBS would benefit from regular MRI examinations, as MRI is often the diagnostic tool of choice to diagnose injury due to trauma or evaluate comorbidities. There are over 75,000 patients with DBS implants worldwide and approximately only one patient over twenty is assessed with MRI. In this pilot study the use of VPS in patients with DBS implants is investigated gathering preliminary results on the anatomical characterization of the OCD target structures for DBS. Within the study high-resolution 7 Tesla and Connectome MRI data were used and electromagnetic simulations for MRI safety were performed. The surgical procedure may introduce structural changes that maybe seen with the MRI once it is found to be safe using the precautionary principle or precautionary approach to risk management states, which is adopted by all safety organizations including the FDA. Using VPN offers an avenue for showing that MRI may be performed conditionally safe, since VPN allows the estimation of safety parameters such as the Specific absorption rate, etc. Furthermore, the proposed new OCD VPS may allow for improved RF power dosimetry on patients with DBS implants undergoing MRI. For example, the proposed VPS could help evaluating the effect of different lead pathway (e.g., use of loops) (Fig. 5). Note that DBS electrodes/leads are very poor receiving coils, since are not tuned coils connected through coaxial cables [52]. Additionally, the VPS could help evaluate safety of patients with DBS implants undergoing MRI when using novel technologies, such as transmit array [34] (Fig. 6). Future OCD patients with DBS implants may profit from the proposed VPS by allowing for a MRI investigation instead of CT.

ACKNOWLEDGMENT

Funding provided by the National Institute of Health, National Institute of Biomedical Imaging and Bioengineering 1R21EB016449-01A1. he mention of commercial products, their sources, or their use in connection with material reported herein is not to be construed as either an actual or implied endorsement of such products by the Department of Health and Human Services.

REFERENCES

[1] G. Bonmassar and N. Makris, "The Virtual Patient Simulator of Deep Brain Stimulation in the Obsessive Compulsive Disorder Based on Connectome and 7 Tesla MRI Data" in - *COGNITIVE 2014, The Sixth International Conference on Advanced Cognitive Technologies and Applications*, Venice, Italy, vol.10, pp.235-238, 2014.

[2] P. R. Arantes, E. F. Cardoso, M. A. Barreiros, M. J. Teixeira, M. R. Goncalves, E. R. Barbosa, *et al.*, "Performing functional magnetic resonance imaging in patients with Parkinson's disease treated with deep brain stimulation," *Mov Disord*, vol. 21, pp. 1154-62, Aug 2006.

[3] F. G. Shellock and A. Spinazzi, "MRI safety update 2008: part 2, screening patients for MRI," *AJR Am J Roentgenol*, vol. 191, pp. 1140-9, Oct 2008.

[4] B. Stevenson, W. Dabney, and C. Frysz, "Issues and design solutions associated with performing MRI scans on patients with active implantable medical devices," *Conf Proc IEEE Eng Med Biol Soc*, vol. 2007, pp. 6167-70, 2007.

[5] K. B. Baker, J. A. Tkach, M. D. Phillips, and A. R. Rezai, "Variability in RF-induced heating of a deep brain stimulation implant across MR systems," *J Magn Reson Imaging*, vol. 24, pp. 1236-42, Dec 2006.

[6] R. Buchli, P. Boesiger, and D. Meier, "Heating effects of metallic implants by MRI examinations," *Magn Reson Med*, vol. 7, pp. 255-61, Jul 1988.

[7] C. K. Chou, J. A. McDougall, and K. W. Chan, "RF heating of implanted spinal fusion stimulator during magnetic resonance imaging," *IEEE Trans Biomed Eng*, vol. 44, pp. 367-73, May 1997.

[8] L. M. Angelone, J. Ahveninen, J. W. Belliveau, and G. Bonmassar, "Analysis of the role of lead resistivity in specific absorption rate for deep brain stimulator leads at 3T MRI," *IEEE Trans Med Imaging*, vol. 29, pp. 1029-38, Apr 2010.

[9] J. Spiegel, G. Fuss, M. Backens, W. Reith, T. Magnus, G. Becker, *et al.*, "Transient dystonia following magnetic resonance imaging in a patient with deep brain stimulation electrodes for the treatment of Parkinson disease. Case report," *J Neurosurg*, vol. 99, pp. 772-4, Oct 2003.

[10] J. M. Henderson, J. Tkach, M. Phillips, K. Baker, F. G. Shellock, and A. R. Rezai, "Permanent neurological deficit related to magnetic resonance imaging in a patient with implanted deep brain stimulation electrodes for Parkinson's disease: case report," *Neurosurgery*, vol. 57, p. E1063; discussion E1063, Nov 2005.

[11] C. Roark, S. Whicher, and A. Abosch, "Reversible neurological symptoms caused by diathermy in a patient with deep brain stimulators: case report," *Neurosurgery*, vol. 62, p. E256; discussion E256, Jan 2008.

[12] D. Shrivastava, A. Abosch, T. Hanson, J. Tian, A. Gupte, P. A. Iaizzo, *et al.*, "Effect of the extracranial deep brain stimulation lead on radiofrequency heating at 9.4 Tesla (400.2 MHz)," *J Magn Reson Imaging*, vol. 32, pp. 600-7, Sep 2010.

[13] Medtronic, "MRI guidelines for Medtronic Deep Brain Stimulation Systems.," 2008.

[14] E. Cabot, T. Lloyd, A. Christ, W. Kainz, M. Douglas, G. Stenzel, *et al.*, "Evaluation of the RF heating of a generic deep brain stimulator exposed in 1.5 T magnetic resonance scanners," *Bioelectromagnetics*, vol. 34, pp. 104-13, Feb 2013.

[15] M. Oliveri, G. Koch, S. Torriero, and C. Caltagirone, "Increased facilitation of the primary motor cortex following 1 Hz repetitive transcranial magnetic stimulation of the contralateral cerebellum in normal humans," *Neurosci Lett*, vol. 376, pp. 188-93, Mar 16 2005.

[16] C. R. Merritt, H. T. Nagle, and E. Grant, "Fabric-Based Active Electrode Design and Fabrication for Health Monitoring Clothing," *Information Technology in Biomedicine, IEEE Transactions on*, vol. 13, pp. 274-280, 2009.

[17] C. R. Butson, S. E. Cooper, J. M. Henderson, and C. C. McIntyre, "Patient-specific analysis of the volume of tissue activated during deep brain stimulation," *Neuroimage*, vol. 34, pp. 661-70, Jan 15 2007.

[18] M. Seyal, A. J. Shatzel, and S. P. Richardson, "Crossed inhibition of sensory cortex by 0.3 Hz transcranial magnetic stimulation of motor cortex," *J Clin Neurophysiol*, vol. 22, pp. 418-21, Dec 2005.

[19] F. Tyc, A. Boyadjian, and H. Devanne, "Motor cortex plasticity induced by extensive training revealed by transcranial magnetic stimulation in human," *Eur J Neurosci*, vol. 21, pp. 259-66, Jan 2005.

[20] M. M. Elwassif, A. Datta, A. Rahman, and M. Bikson, "Temperature control at DBS electrodes using a heat sink: experimentally validated FEM model of DBS lead architecture," *J Neural Eng*, vol. 9, p. 046009, Aug 2012.

[21] M. I. Iacono, N. Makris, L. Mainardi, L. M. Angelone, and G. Bonmassar, "MRI-based multiscale model for electromagnetic analysis in the human head with implanted DBS," *Comput Math Methods Med*, vol. 2013, p. 694171, 2013.

[22] P. Gajsek, T. J. Walters, W. D. Hurt, J. M. Ziriax, D. A. Nelson, and P. A. Mason, "Empirical validation of SAR values predicted by FDTD modeling," *Bioelectromagnetics*, vol. 23, pp. 37-48, Jan 2002.

[23] P. A. Cannistraro, N. Makris, J. D. Howard, M. M. Wedig, S. M. Hodge, S. Wilhelm, *et al.*, "A diffusion tensor imaging study of white matter in obsessive-compulsive disorder," *Depress Anxiety*, vol. 24, pp. 440-6, 2007.

[24] J. F. Lehman, B. D. Greenberg, C. C. McIntyre, S. A. Rasmussen, and S. N. Haber, "Rules ventral prefrontal cortical axons use to reach their targets: implications for diffusion tensor imaging tractography and deep brain stimulation for psychiatric illness," *J Neurosci*, vol. 31, pp. 10392-402, Jul 13 2011.

[25] D. S. Tuch, V. J. Wedeen, A. M. Dale, J. S. George, and J. W. Belliveau, "Conductivity mapping of biological tissue using diffusion MRI," *Ann NY Acad Sci*, vol. 888, pp. 314-316, 1999.

[26] C. Gabriel, S. Gabriel, and E. Corthout, "The dielectric properties of biological tissues: III. Parametric models for the dielectric spectrum of tissues," *Phys. Med. Biol.*, vol. 41, pp. 2271–2293, 1996.

[27] J. A. McNab, B. L. Edlow, T. Witzel, S. Y. Huang, H. Bhat, K. Heberlein, *et al.*, "The Human Connectome Project and beyond: initial applications of 300 mT/m gradients," *Neuroimage*, vol. 80, pp. 234-45, Oct 15 2013.

[28] P. Bernardi, M. Cavagnaro, S. Pisa, and E. Piuzzi, "Specific absorption rate and temperature elevation in a subject exposed in the far-field of radio-frequency sources operating in the 10-900-MHz range," *IEEE Trans Biomed Eng*, vol. 50, pp. 295-304, Mar 2003.

[29] N. Makris, L. Angelone, S. Tulloch, S. Sorg, J. Kaiser, D. Kennedy, *et al.*, "MRI-based anatomical model of the human head for specific absorption rate mapping," *Med Biol Eng Comput*, vol. 46, pp. 1239-51, Dec 2008.

[30] C. K. Chou, H. Bassen, J. Osepchuk, Q. Balzano, R. Petersen, M. Meltz, *et al.*, "Radio frequency electromagnetic exposure: tutorial review on experimental dosimetry," *Bioelectromagnetics*, vol. 17, pp. 195-208, 1996.

[31] P. A. Filipek, C. Richelme, D. N. Kennedy, and V. S. Caviness, Jr., "The young adult human brain: an MRI-based morphometric analysis," *Cereb Cortex*, vol. 4, pp. 344-60, Jul-Aug 1994.

[32] N. Makris, J. W. Meyer, J. F. Bates, E. H. Yeterian, D. N. Kennedy, and V. S. Caviness, "MRI-Based topographic parcellation of human cerebral white matter and nuclei II. Rationale and applications with systematics of cerebral connectivity," *Neuroimage*, vol. 9, pp. 18-45, 1999.

[33] Available: http://www.fda.gov/MedicalDevices/ProductsandMedicalProcedures/DeviceApprovalsandClearances/Recently-ApprovedDevices/ucm125520.htm

[34] L. M. Angelone, N. Makris, C. E. Vasios, L. Wald, and G. Bonmassar, "Effect of transmit array phase relationship on local Specific Absorption Rate (SAR)." in *ISMRM Fourteenth Scientific Meeting*, Seattle, USA, 2006.

[35] T. Eichele, S. Debener, V. D. Calhoun, K. Specht, A. K. Engel, K. Hugdahl, *et al.*, "Prediction of human errors by maladaptive changes in event-related brain networks," *Proc Natl Acad Sci U S A*, vol. 105, pp. 6173-8, Apr 22 2008.

[36] C. Gabriel, S. Gabriel, and E. Corthout, "The dielectric properties of biological tissues: I. Literature survey," *Phys. Med. Biol.*, vol. 41, pp. 2231–2249, 1996.

[37] C. Gabriel, S. Gabriel, and E. Corthout, "The dielectric properties of biological tissues: II. Measurements in the frequency range 10 Hz to 20 GHz," *Phys. Med. Biol.*, vol. 41, pp. 2251–2269, 1996.

[38] L. M. Angelone, E. Eskandar, and G. Bonmassar, "Resistive tapered stripline for deep brain stimulation (DBS) leads at 7 T MRI: Specific absorption rate analysis with high-resolution head model.," in *The 24th Progress in Electromagnetics Research Symposium (PIERS)*, Cambridge, MA, USA, 2008.

[39] W. R. Nitz, G. Brinker, D. Diehl, and G. Frese, "Specific absorption rate as a poor indicator of magnetic resonance-related implant heating," *Invest Radiol*, vol. 40, pp. 773-6, Dec 2005.

[40] IEC, "International Standard, medical equipment - 60601-2-33: Particular requirements for the safety of the magnetic resonance equipment for medical diagnosis, 2nd revision," Geneva2010.

[41] H. M. Duvernoy, *Human brain stem vessels : including the pineal gland and information on brain stem infarction*, 2nd completely rev. and expanded ed. Berlin ; New York: Springer, 1999.

[42] H. M. Duvernoy, *The human brain stem and cerebellum. surface, structure, vascularization, and three-dimensional sectional anatomy with MRI*. New York, 1995.

[43] H. M. Duvernoy, S. Delon, and J. L. Vannson, "Cortical blood vessels of the human brain," *Brain Res Bull*, vol. 7, pp. 519-79, Nov 1981.

[44] G. Schaltenbrand and P. Bailey, *Einführung in die stereotaktischen Operationen, mit einem Atlas des menschlichen Gehirns. Introduction to stereotaxis, with an atlas of the human brain*. Stuttgart,: G. Thieme, 1959.

[45] S. Pallanti and L. Quercioli, "Treatment-refractory obsessive-compulsive disorder: methodological issues, operational definitions and therapeutic lines," *Prog Neuropsychopharmacol Biol Psychiatry*, vol. 30, pp. 400-12, May 2006.

[46] D. D. Dougherty, L. Baer, G. R. Cosgrove, E. H. Cassem, B. H. Price, A. A. Nierenberg, *et al.*, "Prospective long-term follow-up of 44 patients who received cingulotomy for treatment-refractory obsessive-compulsive disorder," *Am J Psychiatry*, vol. 159, pp. 269-75, Feb 2002.

[47] H. H. Jung, C. H. Kim, J. H. Chang, Y. G. Park, S. S. Chung, and J. W. Chang, "Bilateral anterior cingulotomy for refractory obsessive-

compulsive disorder: Long-term follow-up results," *Stereotact Funct Neurosurg*, vol. 84, pp. 184-9, 2006.

[48] P. K. Bridges, J. R. Bartlett, A. S. Hale, A. M. Poynton, A. L. Malizia, and A. D. Hodgkiss, "Psychosurgery: stereotactic subcaudate tractomy. An indispensable treatment," *Br J Psychiatry*, vol. 165, pp. 599-611; discussion 612-3, Nov 1994.

[49] A. D. Hodgkiss, A. L. Malizia, J. R. Bartlett, and P. K. Bridges, "Outcome after the psychosurgical operation of stereotactic subcaudate tractotomy, 1979-1991," *J Neuropsychiatry Clin Neurosci*, vol. 7, pp. 230-4, Spring 1995.

[50] S. K. Bourne, A. Conrad, J. S. Neimat, and T. L. Davis, "Linear measurements of the cerebral ventricles are correlated with adult ventricular volume," *J Clin Neurosci*, vol. 20, pp. 763-4, May 2013.

[51] L. Yang, A. V. Sycheva, D. M. Black, and R. Eastell, "Site-specific differential effects of once-yearly zoledronic acid on the hip assessed with quantitative computed tomography: results from the HORIZON Pivotal Fracture Trial," *Osteoporos Int*, vol. 24, pp. 329-38, Jan 2013.

[52] E. Atalar, "Catheter Coils," in *eMagRes*, ed: John Wiley & Sons, Ltd, 2007.